

Article

Structural and Mechanical Properties of Arc-Sprayed Ni–Cr Coating Post-Treated by Surface Mechanical Attrition Treatment (SMAT)

Karima Aoudia ^{1,2,3,*}, Salim Lamri ^{1,2}, Sofiane Achache ^{1,2}, Delphine Retraint ¹,
Christophe Verdy ⁴ , Cécile Langlade ⁴, Said Azem ³ and Frédéric Sanchette ^{1,2} 

¹ ICD, P2MN, LASMIS, Université de Technologie de Troyes (UTT), CNRS, 10000 Troyes, France; salim.lamriutt@gmail.com (S.L.); sofiane.achache@utt.fr (S.A.); delphine.retraint@utt.fr (D.R.); frederic.sanchette@utt.fr (F.S.)

² Nogent International Center for CVD Innovation (NICCI), LRC CEA-ICD LASMIS, UTT Antenne de Nogent, pôle technologique de haute Champagne, 52800 Nogent, France

³ LEC2M, Université Mouloud Mammeri de Tizi-Ouzou, B.P. 17, Hasnaoua, 15000 Tizi-Ouzou, Algérie; said.azem@ummto.dz

⁴ Université Bourgogne Franche Comté, ICB UMR 6303 CNRS, site UTBM, 90100 Belfort, France; christophe.verdy@utbm.fr (C.V.); cecile.langlade@utbm.fr (C.L.)

* Correspondence: karima.aoudia@utt.fr

Received: 1 October 2018; Accepted: 19 November 2018; Published: 26 November 2018



Abstract: This study focuses on the effects of a surface mechanical attrition treatment on the structural and mechanical behavior of arc-sprayed Ni–Cr coatings deposited on steel substrates. The surface of the as-sprayed and SMATed coatings was characterized by X-ray diffraction, Scanning Electron Microscopy, and non-contact profilometry. The coating porosity was evaluated by using image analysis software. The residual stresses were determined using X-ray diffraction with the $\sin^2\psi$. Indentation tests were carried out on the cross sections of the different coatings to evaluate their hardness. The wear properties of the coatings were assessed using a pin-on-disk tester at ambient temperature without lubrication. The results showed that surface mechanical attrition treatment (SMAT) induced a grain refinement on the coating surface due to severe plastic deformation, which was associated with a significant improvement of the mechanical properties.

Keywords: arc spraying; surface mechanical attrition treatment (SMAT); Ni-based coating

1. Introduction

Nickel-based coatings are currently used for many applications in the surface treatment of metallic components to improve their resistance against wear and corrosion in the chemical and mechanical industries.

Several thermal spray methods have been used to deposit Ni-based coatings, among which, the most used techniques are: plasma spraying [1–4], high-velocity air-fuel spraying [5,6], high-velocity oxy-fuel spraying [4,6–8], arc spraying [9,10], and cold spraying [11]. The principle of the thermal spraying technique consists in using a source of energy to heat and melt the coating materials and then accelerate and deposit them on the substrate.

The characteristics and performances of the resulting coatings are strongly affected by the presence of defects, which correspond to partly and fully melted particles with oxides, cracks, and porosity, as well as residual stresses [3,12–17].

Previous studies have been performed to explore the effect of different spraying conditions on the structural and mechanical properties of thermally sprayed coatings [11,18–21]. It has been

demonstrated that porosity and defects contents in the thermally sprayed coatings can be controlled by changing several process parameters, such as spraying angle, particle velocity, temperature at impact, and spray distance.

Many studies [22–28] focused on the effects of heat treatments on the microstructure and mechanical properties evolution of thermally sprayed Ni-based coatings. It was shown that coatings heat-treated at 700 and 900 °C have a dense structure and low porosity. However, the heat treatment has no important influence on the friction coefficient and wear resistance.

Several methods have been carried out to improve the characteristics of thermally sprayed coatings. Laser melting is one of the most used techniques [10,29–35]. The process is able to reduce the porosity and interlamellar structure in the coatings and leads to an improvement of their wear and corrosion resistance. Nevertheless, during this process, a strong rise in temperature occurs that can induce thermal stresses, which lead to cracks in the laser-treated coatings.

In this work, surface mechanical attrition treatment (SMAT) was chosen as a post-treatment performed on a Ni–Cr thermally sprayed coating. SMAT is actually a mechanical surface treatment derived from shot peening which can enhance corrosion resistance [36–38], tensile [39,40], fatigue [41,42], or tribological properties [43–45]. Tchana Nkonta et al. [38] studied the influence of SMAT on the corrosion behavior of a Co–Cr–Mo alloy through potentiodynamic measurements and electrochemical impedance spectroscopy. The results revealed that SMAT promotes passive film formation and increases corrosion resistance in Ringer’s solution. Chen et al. [39] investigated the effect of SMAT on the tensile properties of nanocrystalline 316L austenitic stainless steel. The results showed that the SMATed materials exhibit a high strength up to 1450 MPa, which is six times higher than that of the initial material. Alikhani et al. [44] investigated the effect of the grain size of SMATed pure titanium (Cp-Ti) on wear resistance. The results indicated that SMAT decreased the friction coefficient by about 66%.

SMAT is based on the motion of perfectly spherical balls placed in a cylindrical chamber. The bottom of the chamber (called sonotrode) is put into vibration using an ultrasonic generator. The repeated impacts of the balls on the sample surface usually generate severe plastic deformation as well as the formation of a superficial nanocrystalline layer [46,47]. Liu et al. [47] obtained a nanocrystalline layer in pure Al by means of SMAT. They explained, by TEM analyses, that dislocation slips was the main mechanism of grain refinement of Al. SMAT also generates compressive residual stress on the surface of the treated part [43,48]. Zhou et al. [48] studied the effects of SMAT and conventional shot peening (CSP) on the surface low-cycle fatigue (LCF) properties of 316L. They found that the fatigue life of the materials treated by CSP was higher than that of materials treated by SMAT under a low strain amplitude. The authors attributed this to the fact that the compressive residual stress was higher for the samples treated by CSP than for those treated by SMAT. In contrast, under a higher strain amplitude, the fatigue life of the samples treated with CSP was lower than that of the samples subjected to SMAT, which was due to a quick relaxation of residual stress under high strain amplitude. In this study, SMAT was performed as a post-treatment and was expected to reduce coating porosity and defects contents as well as to enhance their mechanical properties.

A Ni–Cr coating was sprayed on E355 steel using a twin wire electric arc spraying and then was subjected to SMAT. The effects of SMAT parameters, especially the amplitude of vibration and the duration of the treatment, on the mechanical and structural properties of the coating were investigated in order to limit the cracks and the porosity in the SMATed coating. The relationships between microstructure and mechanical properties were also analyzed.

2. Experimental Details

2.1. Material

Nickel–Chromium wires 80/20 (at.%) with a 1.6 mm diameter were used for arc spraying. Before deposition, the E355 steel substrates were degreased with alcohol and grit-blasted with corundum F60 (250 μm) to provide a rough surface for better adhesion by removing all rust and oxides. The arc spraying was conducted on a twin wire arc gun system (Tafa 9000 model, Praxair Surface Technologies, Indianapolis, IN, USA) with a robot control system (ABB 4400, Société helvético-suédoise, Zurich, Switzerland). The twin wire arc spraying parameters are detailed in Table 1.

Table 1. Arc spraying parameters.

Spraying Parameters	Value
Arc current (A)	135
Arc voltage (V)	33
Spray distance (mm)	125
Spray speed (mm/s)	500
Pressure of compressed air (bar)	8.25
Nitrogen flow rate (m^3/h)	42–50
Spray passes	8
Steps (mm)	8

2.2. Surface Mechanical Attrition Treatment (SMAT)

SMAT was performed at ambient temperature in air using 3 mm diameter spherical 100Cr6 balls. A vibration frequency of the sonotrode of 20 kHz was imposed. The different studied SMAT conditions are summarized in Table 2.

Table 2. Surface Mechanical Attrition Treatment (SMAT) parameters.

Specimen Label	Nature of Balls	Diameter of Balls (mm)	Amplitude of Vibration (μm)	Treatment Duration (s)
NS	–	–	–	–
S 15-01	100Cr6	3	15	405
S 15-02	–	–	–	810
S 25-01	–	–	25	400
S 25-02	–	–	–	800

2.3. Structural Analysis

The surface and cross-section morphology of the coatings were analyzed at 20 kv using an HIROX SH-4000 Scanning Electron Microscope (SEM, Synergie4, Lisses, France) equipped with an EDS-X system. The porosity was measured on SEM images using Image analysis software; for each sample, 10 measurements were performed, and the measurement values were averaged. The phase structure of the coatings was assessed by X-ray diffraction analysis (BRUKER D8 ADVANCED, BRUKER, Karlsruhe, Germany) with $\text{CuK}\alpha$ radiation (0.15418 nm) generated at 40 kV and 40 mA. The diffraction angle 2θ ranged from 20° to 120° .

The surface roughness values (R_a) of the coatings was measured using an AltiSurf[®]500 non-contact profilometer (Physical Test Solutions, Culver City, CA, USA).

2.4. Mechanical Properties

The elastic modulus and hardness of the coating before and after SMAT were measured from the polished cross-sectional surface by Nano Indenter XP, MTS System Corporation (Eden Prairie, MN, USA), with a continuous stiffness technique (CSM) and equipped with a Berkovitch indenter.

The tip was calibrated by indenting in a standard fused silica calibration specimen, following the Olivier & Pharr calibration procedure (Oliver_1992). This calibration was adapted to the present working depth. A total of 49 indentations were made, the Young's modulus and hardness were calculated from the Olivier Pharr model [49], and the results were averaged.

Residual stresses in the coating before and after SMAT were investigated by X-ray diffraction using the $\sin^2\psi$ method. Strain measurement were performed on the (311) Bragg peak obtained at $2\theta = 92^\circ$. The collimator size was 1 mm. The samples were tilted between 0° and 70° with a step of 10 for the ψ scan. Measurements were taken at five different orientations ($\phi = 0^\circ$, $\phi = 45^\circ$, $\phi = 90^\circ$, $\phi = 180^\circ$, $\phi = 225^\circ$) for the ϕ scan. In order to calculate residual stresses, the data were analyzed using Leptos software version 7.8 as part of Bruker AXS Suite software.

Tribological tests on the coated samples (40 mm diameter) were conducted using an Anton Paar tribometer (Pesex, Switzerland) with ball on disk configuration. The tests were carried out at room temperature without lubrication. A 100Cr6 steel ball with a diameter of 6 mm was chosen as the counterpart material. The sliding tests were conducted at a normal load of 5 N and a sliding distance of 200 m. The friction coefficient was recorded automatically using a computer connected to the wear tester. The wear volume loss was measured using a 3D profilometer. The wear rate was calculated as $W = \frac{V}{L \cdot S}$, where V is the wear volume loss in mm^3 , S is the total sliding distance (m), and L is the normal load (N). The wear test conditions are listed in Table 3.

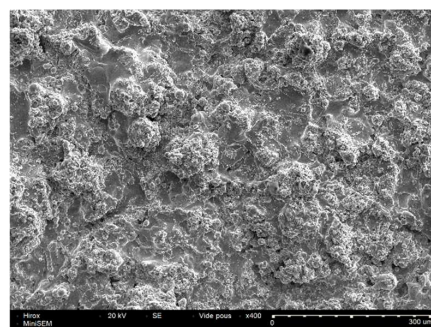
Table 3. Wear tests conditions (ball-on-disk tests).

Parameters	Values
Ball material	100Cr6
Ball diameter (mm)	6
Load (N)	5
Radius (mm)	6
Linear speed (m/s)	0.1
Sliding distance (m)	200
Temperature ($^\circ\text{C}$)	23

3. Results and Discussion

3.1. Morphology

The surface morphologies of as-deposited and SMATed coatings at different parameters are shown in Figure 1. The morphology of the as-sprayed coating consisted of interlocked particles with irregular morphologies. Molten, partially melted, and unmelted particles were observed on the surface of the as-deposited coatings, which contributed to generate porosities and led to a very rough surface. Some micro-cracks were also found throughout the particles. The surface of the SMATed coatings was more compact and smoother. The numbers of voids and pores decreased significantly on the top surface with the increase of the amplitude of vibration and the duration of the SMAT process.



(a)

Figure 1. Cont.

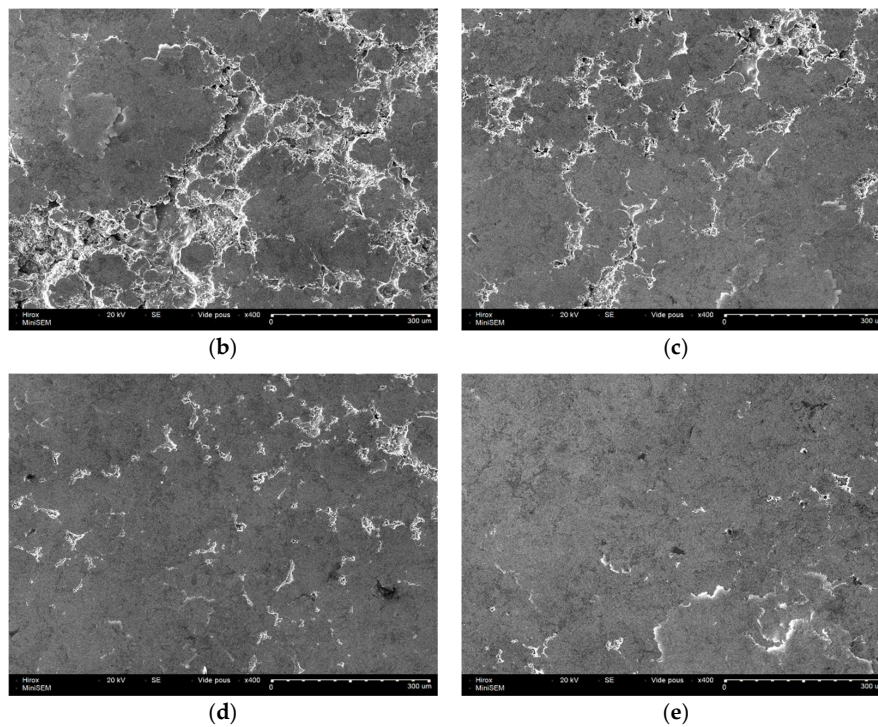


Figure 1. SEM micrographs of coatings' surfaces: (a) Untreated Ni–Cr; (b) SMATed with an amplitude of 15 μm for 405 s; (c) SMATed with an amplitude of 15 μm for 810 s; (d) SMATed with an amplitude of 25 μm for 400 s; (e) SMATed with an amplitude of 25 μm for 800 s.

Cross sections of the as-sprayed and SMATed coatings corresponding to various parameters are shown in Figure 2. It is shown that the as-deposited coatings had a lamellar structure containing pores and interlamellar cracks. The formation of interlamellar cracks was due to the thermal stress caused by rapid solidification. After SMAT, the coatings were more compact, without defects or cracks.

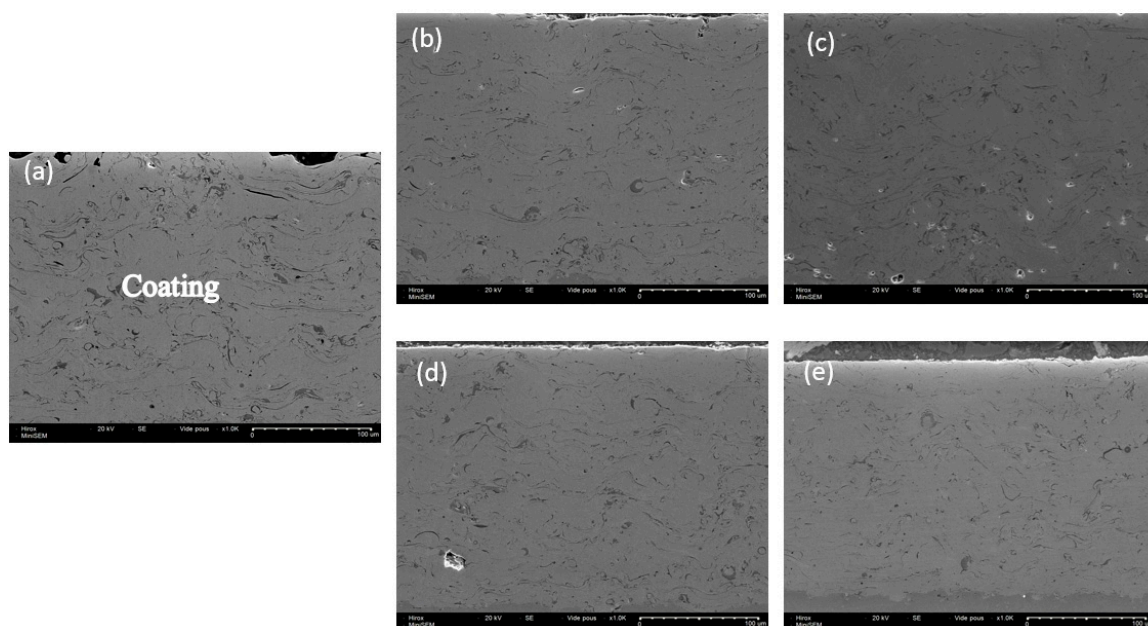


Figure 2. Cross-sectional morphology of 80Ni–20Cr coating: (a) Untreated Ni–Cr; (b) SMATed with an amplitude of 15 μm for 405 s; (c) SMATed with an amplitude of 15 μm for 810 s; (d) SMATed with an amplitude of 25 μm for 400 s; (e) SMATed with an amplitude of 25 μm for 800 s.

The thickness evolution as a function of the duration of SMAT treatment is shown Figure 3. A slight decrease in the coating thickness was observed when the duration of SMAT rose. This evolution could be attributed to the more compact coating morphology and to the decrease in roughness, which can influence the thickness measurements.

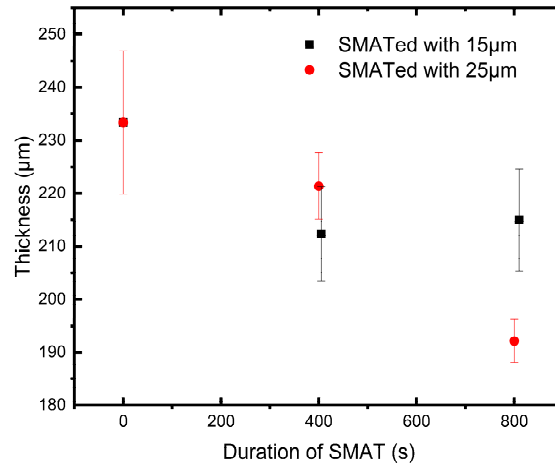


Figure 3. Coating thickness as a function of SMAT duration and amplitude.

Coating porosity is measured on the cross-section before and after SMAT using “ImageJ” software (version 1.45). Figure 4 reports the results of porosity rate value as a function of SMAT parameters. Porosities values of the coatings decreased from 5.95% for the untreated coating to 0.83% for the coating SMATed with an amplitude of 25 µm for 800 s. The porosity’s rate decreases with an increase of the amplitude of vibration as well as of the SMAT duration. This result is consistent with that of the Figure 3.

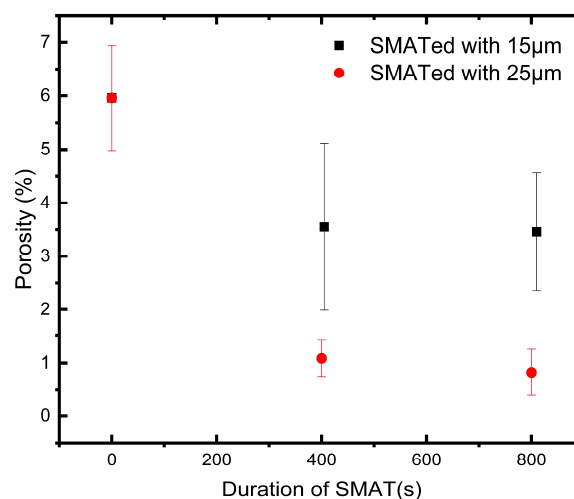


Figure 4. Coating porosity as a function of SMAT duration and amplitude.

3.2. Roughness

The surface roughness of the samples was evaluated using an AltiSurf[®]500 profilometer. The results were analyzed using Altimet software (version 7.1). The measured values of R_a (Figure 5) showed that the as-deposited coating surface was irregular and had a high roughness, with an R_a of 11.85 µm. The SMATed samples had a smoother surface with a lower R_a value of 1.43 µm. Balls imprints were also noticeable after SMAT, as a result of plastic deformation occurring during the SMAT process.

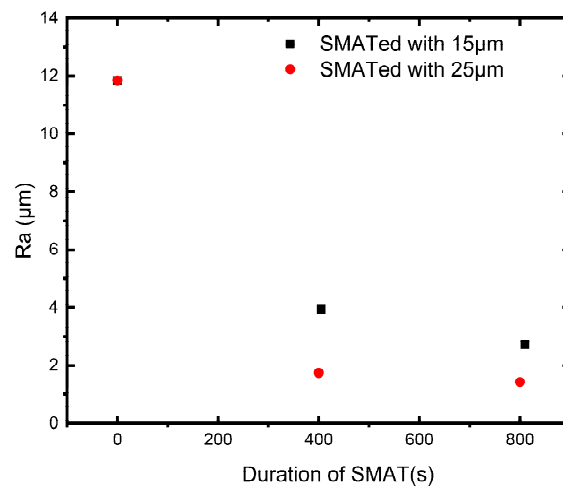


Figure 5. Surface roughness evolution as a function of SMAT duration and amplitude of vibration.

3.3. Structure

The X-ray diffraction (XRD) patterns of the coatings treated at different SMAT parameters are shown in Figure 6. All the coatings were face centered cubic (FCC) single-phased and consisted of a γ Ni-(Cr) solid solution.

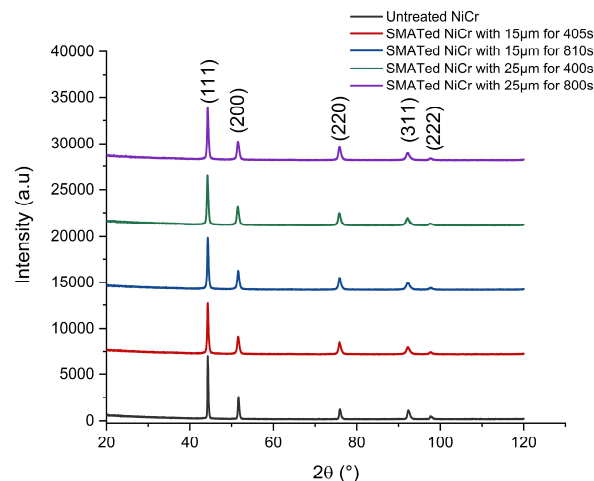


Figure 6. X-ray diffraction patterns of Ni-Cr coatings before and after SMAT at different conditions.

Figure 7 shows a broadening and slight shift of the diffraction peaks after SMAT, which can be attributed to a grain refinement and micro-strain induced by balls' impacts.

The mean grain size and micro-strains of the coatings before and after SMAT were calculated from the XRD patterns using MAUD software (version 2.80). Figure 8 shows that an increase in SMAT duration and amplitude of vibration led to a decrease of the mean grain size and to an increase of the micro-strain. The micro-strain value in the as-deposited coating was 0.0016, suggesting that the arc thermally sprayed coating contained micro-strain and defects. This parameter reached 0.0027 (almost the double of the previous value) for the sample SMATed with amplitude of vibration of 25 μ m for 400 s, which can be explained by micro-deformation of the crystallites induced by plastic deformation. The reduction in mean grain size with increasing SMAT duration was obviously due to the accumulation of plastic deformation and strain in the superficial area [50–54].

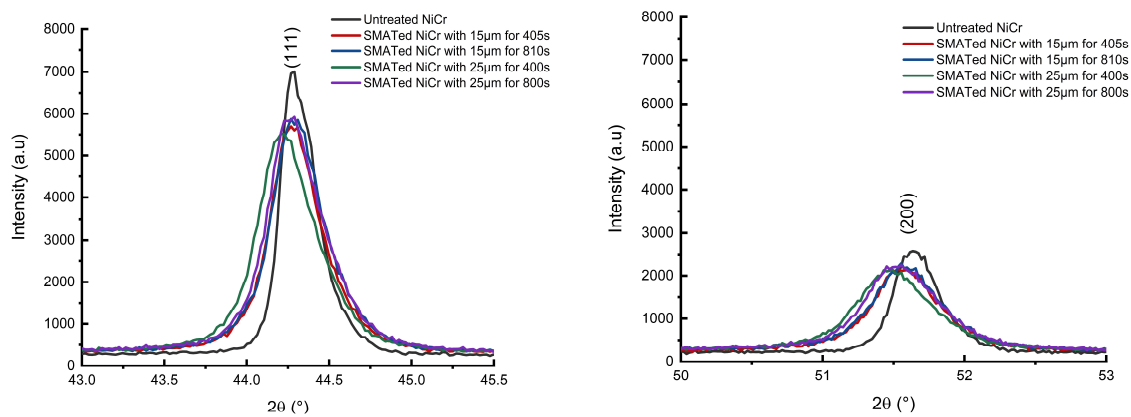


Figure 7. Zoomed images of the XRD patterns of Figure 6.

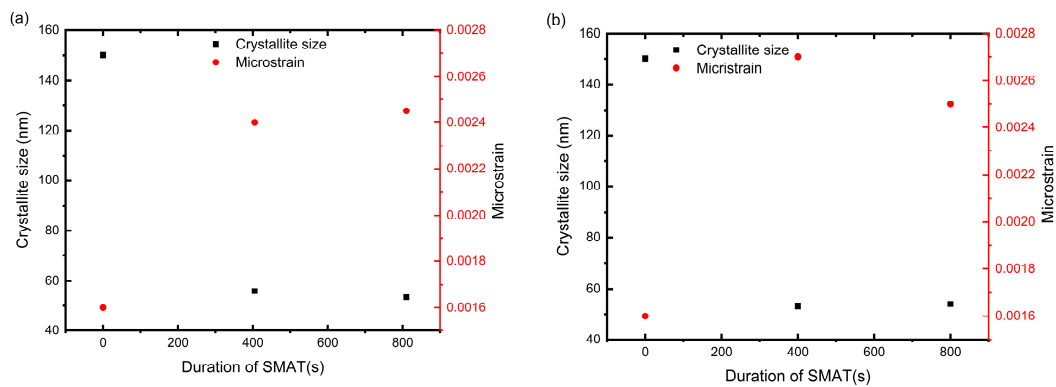


Figure 8. Mean grain size and micro-strain evolution as a function of SMAT duration; (a) SMATed with an amplitude of 15 µm; (b) SMATed with an amplitude of 25 µm.

3.4. Nano Indentation

Figure 9a,b show the evolution of both the hardness H and the Young's modulus as a function of SMAT duration. It is clearly shown that SMAT favored an increase of both hardness and elastic modulus. Indeed, hardness and Young's modulus reached a maximum value of 5.36 and 218 GPa, respectively after SMAT, while values of 4.56 and 176 GPa were measured for the untreated coating. The increase in hardness and Young's modulus can be explained by grain refinement and high compressive residual stresses (Section 3.5), associated with a more compact morphology, resulting from balls' impacts during SMAT. Thus, the coatings exhibited better mechanical properties after SMAT.

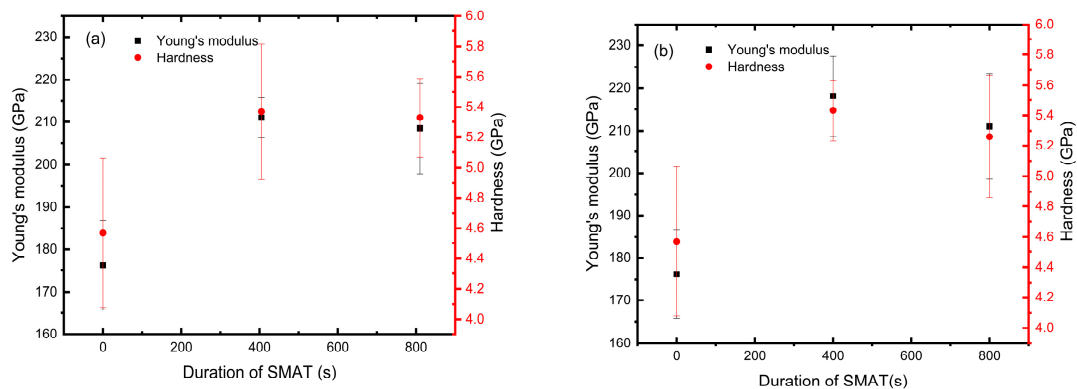


Figure 9. Young's modulus and hardness evolution of Ni-Cr coatings as a function of SMAT duration: (a) SMATed with an amplitude of 15 µm; (b) SMATed with an amplitude of 25 µm.

3.5. Residual Stresses

Figure 10 displays a comparison between the measured residual stresses values of the as-deposited and SMATed coatings. The surface residual stresses of the as-sprayed coatings were tensile and were generated by the deposition process [15,18,21,55] and from the difference in the coefficients of thermal expansion between the coatings and the substrate [56,57].

The residual stresses changed significantly from tensile to compression by increasing the amplitude of vibration and SMAT duration. This could be attributed to the distortion of the crystalline lattice and to the generation of dislocations by severe plastic deformation during SMAT. This result is very interesting from the point of view of mechanical applications.

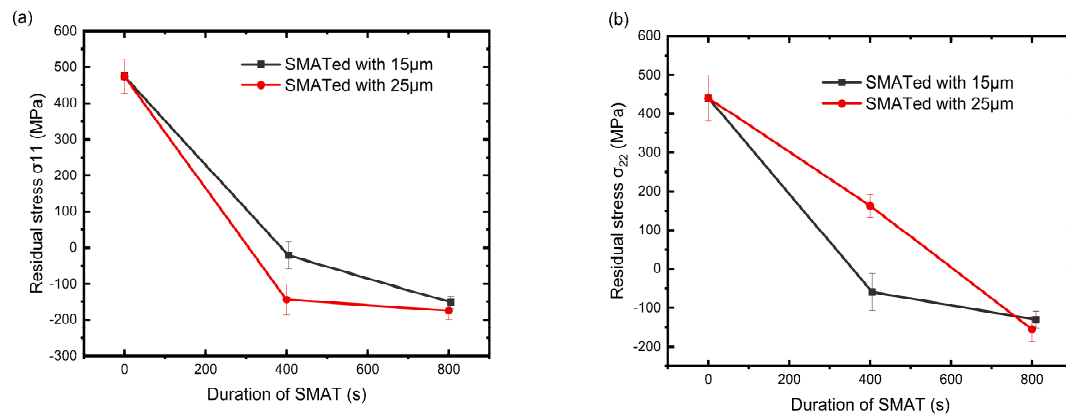


Figure 10. Residual stress evolution of Ni–Cr coatings as a function of SMAT duration: (a) σ_{11} ; (b) σ_{22} .

3.6. Friction and Wear Resistance

Figure 11 shows the variation of the friction coefficient as a function of the sliding distance for various SMAT parameters. All values of the friction coefficient were in the range between 0.65 and 0.85, comparable to the friction coefficient of the Ni–Cr as-deposited coating.

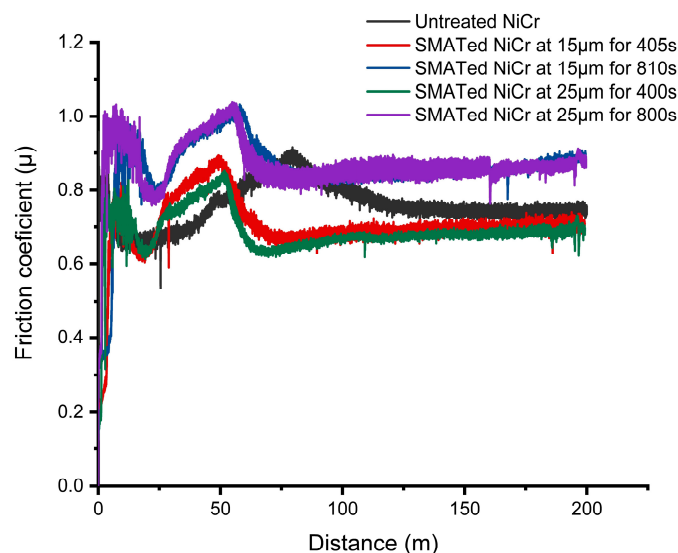


Figure 11. Friction coefficient of the coatings in different SMAT conditions.

The effect of SMAT on the wear rate is shown in Figure 12. It is clear that the wear rate decreased with the increase of the amplitude of vibration and the duration of the SMAT process. In particular, the coating treated with amplitude of 25 µm for 800 s was found to exhibit a wear resistance 80% higher than that of the as-deposited coating. The improvement in wear resistance could be related to

SMAT-induced grain refinement associated with a higher hardness, which led to a decrease of the wear rate. Thus, grain refinement resulting from plastic deformation associated with compressive residual stress induced a higher hardness of the coatings, which improved the wear resistance.

Moreover, the decrease of the roughness observed when the amplitude of vibration and duration of the SMAT increased favored low wear rates.

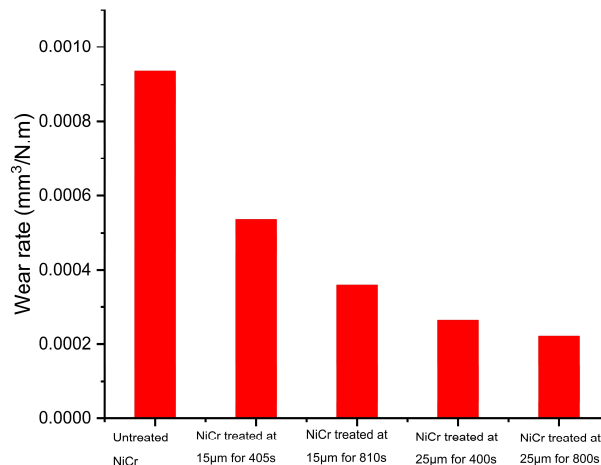


Figure 12. Wear rate of the coatings in different SMAT conditions.

4. Conclusions

The effects of SMAT parameters (amplitude of vibration and duration) on the structural and mechanical behavior of a thermally sprayed Ni–Cr coating deposited on steel substrates were investigated.

SMAT improved the performances of the as-sprayed coating by reducing its surface roughness as well as by eliminating its porosities and lamellar morphology.

Severe plastic deformation generated by SMAT led to a grain refinement phenomenon and induced compressive residual stresses in the SMATed materials, which was associated with an increase of hardness and Young’s modulus of the coating. Consequently, the wear resistance was significantly increased by SMAT.

SMAT seems to be a particularly interesting treatment to optimize the morphology, structure, mechanical characteristics, and, therefore, performances of the coatings obtained by spray technologies.

Author Contributions: Conceptualization, K.A.; Funding Acquisition, K.A., D.R. and F.S.; Methodology, K.A., S.L., S.A. (Sofiane Achache), D.R., C.V., C.L., S.A. (Said Azem) and F.S.; Software, S.L., S.A. (Sofiane Achache) and C.V.; Supervision, S.A. (Said Azem) and F.S.; Validation, D.R., S.A. (Said Azem) and F.S.; Writing–Original Draft, K.A.

Funding: This research received no external funding.

Acknowledgments: The authors acknowledge “la Région Champagne-Ardenne” European Funds for Regional Development (FEDER) for financial support through the project ECOPHY.

Conflicts of Interest: The authors declare no conflict of interest.

References

- Vicenzi, J.; Marques, C.M.; Bergmann, C.P. Hot and cold erosive wear of thermal sprayed NiCr-based coatings: Influence of porosity and oxidation. *Surf. Coat. Technol.* **2008**, *202*, 3688–3697. [[CrossRef](#)]
- Du, L.; Huang, C.; Zhang, W.; Li, T.; Liu, W. Preparation and wear performance of NiCr/Cr₃C₂–NiCr/hBN plasma sprayed composite coating. *Surf. Coat. Technol.* **2011**, *205*, 3722–3728. [[CrossRef](#)]
- Ivannikov, A.Y.; Kalita, V.I.; Komlev, D.I.; Radyuk, A.A.; Bagmutov, V.P.; Zakharov, I.N.; Parshev, S.N. The effect of electromechanical treatment on structure and properties of plasma sprayed Ni-20Cr coating. *J. Alloy. Compd.* **2016**, *655*, 11–20. [[CrossRef](#)]

4. Lin, L.; Lia, G.-L.; Wang, H.-D.; Kang, J.-J.; Xu, Z.-L.; Wang, H.-J. Structure and wear behavior of NiCr-Cr₃C₂ coatings sprayed by supersonic plasma spraying and high velocity oxy-fuel technologies. *Appl. Surf. Sci.* **2015**, *356*, 383–390. [[CrossRef](#)]
5. Sadeghimeresht, E.; Markocsan, N.; Joshi, S. Isothermal oxidation behavior of HVOF-sprayed Ni and NiCr coatings in H₂-H₂O environment. *Surf. Coat. Technol.* **2017**, *317*, 17–25. [[CrossRef](#)]
6. Bolelli, G.; Berger, L.M.; Börner, T.; Koivuluoto, H.; Matikainen, V.; Lusvarghi, L.; Lyphout, C.; Markocsan, N.; Nylén, P.; Sassatelli, P.; et al. Sliding and abrasive wear behavior of HVOF-and HVOF-sprayed Cr₃C₂-NiCr hardmetal coatings. *Wear* **2016**, *358*, 32–50. [[CrossRef](#)]
7. Zhou, W.; Zhou, K.; Li, Y.; Deng, C.; Zeng, K. High temperature wear performance of HVOF-sprayed Cr₃C₂-WC-NiCoCrMo and Cr₃C₂-NiCr hardmetal coatings. *Appl. Surf. Sci.* **2017**, *416*, 33–44. [[CrossRef](#)]
8. Deesom, D.; Charoenrut, K.; Moonngam, S.; Banjongprasert, C. Fabrication and properties of NiCr/CNTs nanocomposite coatings prepared by High Velocity Oxy-Fuel Spraying. *Surf. Coat. Technol.* **2016**, *306*, 240–244. [[CrossRef](#)]
9. Lin, J.; Wang, Z.; Lin, P.; Cheng, J.; Zhang, X.; Hong, S. Effects of post annealing on the microstructure, mechanical properties and cavitation erosion behavior of arc-sprayed FeNiCrBSiNbW coatings. *Mater. Des.* **2015**, *65*, 1035–1040. [[CrossRef](#)]
10. Park, I.C.; Kim, S.J. Corrosion behavior in seawater of arc thermal sprayed Inconel 625 coatings with sealing treatment. *Surf. Coat. Technol.* **2017**, *325*, 729–737. [[CrossRef](#)]
11. Luo, X.T.; Li, Y.J.; Li, C.X.; Yang, G.J.; Li, C.J. Effect of spray conditions on deposition behavior and microstructure of cold sprayed Ni coatings sprayed with a porous electrolytic Ni powder. *Surf. Coat. Technol.* **2016**, *289*, 85–93. [[CrossRef](#)]
12. Chatha, S.S.; Sidhu, H.S.; Sidhu, B.S. High temperature hot corrosion behaviour of NiCr and Cr₃C₂-NiCr coatings on T91 boiler steel in an aggressive environment at 750 °C. *Surf. Coat. Technol.* **2012**, *206*, 3839–3850. [[CrossRef](#)]
13. Khaled, M.M.; Yilbas, B.S. Corrosion properties of HVOF-coated steel in simulated concrete pore electrolyte and concentrated chloride environments. *Surf. Coat. Technol.* **2007**, *202*, 433–438. [[CrossRef](#)]
14. Ahmed, N.; Bakare, M.S.; McCartney, D.G.; Voisey, K.T. The effects of microstructural features on the performance gap in corrosion resistance between bulk and HVOF sprayed Inconel 625. *Surf. Coat. Technol.* **2010**, *204*, 2294–2301. [[CrossRef](#)]
15. Wenzelburger, M.; López, D.; Gadow, R. Methods and application of residual stress analysis on thermally sprayed coatings and layer composites. *Surf. Coat. Technol.* **2006**, *201*, 1995–2001. [[CrossRef](#)]
16. Shukla, V.N.; Jayaganthan, R.; Tewari, V.K. Degradation behavior of HVOF-sprayed Cr₃C₂-25%NiCr cermet coatings exposed to high temperature environment. *Mater. Today Proc.* **2015**, *2*, 1805–1813. [[CrossRef](#)]
17. Nayebpashae, N.; Seyedein, S.H.; Aboutalebi, M.R.; Sarpoolaky, H.; Hadavi, S.M.M. Finite element simulation of residual stress and failure mechanism in plasma sprayed thermal barrier coatings using actual microstructure as the representative volume. *Surf. Coat. Technol.* **2016**, *291*, 103–114. [[CrossRef](#)]
18. Selvadurai, U.; Hollingsworth, P.; Baumann, I.; Hussong, B.; Tillmann, W.; Rausch, S.; Biermann, D. Influence of the handling parameters on residual stresses of HVOF-sprayed WC-12Co coatings. *Surf. Coat. Technol.* **2015**, *268*, 30–35. [[CrossRef](#)]
19. Rajasekaran, B.; Mauer, G.; Vaßen, R.; Röttger, A.; Weber, S.; Theisen, W. Thick tool steel coatings using HVOF spraying for wear resistance applications. *Surf. Coat. Technol.* **2010**, *205*, 2449–2454. [[CrossRef](#)]
20. Pukasiewicz, A.G.M.; de Boer, H.E.; Sucharski, G.B.; Vaz, R.F.; Procopiak, L.A.J. The influence of HVOF spraying parameters on the microstructure, residual stress and cavitation resistance of FeMnCrSi coatings. *Surf. Coat. Technol.* **2017**, *327*, 158–166. [[CrossRef](#)]
21. Katranidis, V.; Gu, S.; Allcock, B.; Kamnis, S. Experimental study of high velocity oxy-fuel sprayed WC-17Co coatings applied on complex geometries. Part A: Influence of kinematic spray parameters on thickness, porosity, residual stresses and microhardness. *Surf. Coat. Technol.* **2017**, *311*, 206–215. [[CrossRef](#)]
22. Chatha, S.S.; Sidhu, H.S.; Sidhu, B.S. The effects of post-treatment on the hot corrosion behavior of the HVOF-sprayed Cr₃C₂-NiCr coating. *Surf. Coat. Technol.* **2012**, *206*, 4212–4224. [[CrossRef](#)]
23. Liu, L.; Xu, H.; Xiao, J.; Wei, X.; Zhang, G.; Zhang, C. Effect of heat treatment on structure and property evolutions of atmospheric plasma sprayed NiCrBSi coatings. *Surf. Coat. Technol.* **2017**, *325*, 548–554. [[CrossRef](#)]

24. Li, G.J.; Li, J.; Luo, X. Effects of high temperature treatment on microstructure and mechanical properties of laser-clad NiCrBSi/WC coatings on titanium alloy substrate. *Mater. Charact.* **2014**, *98*, 83–92. [[CrossRef](#)]
25. Staia, M.H.; Suárez, M.; Chicot, D.; Lesage, J.; Iost, A.; Puchi-Cabrera, E.S. Cr₂C₃-NiCr VPS thermal spray coatings as candidate for chromium replacement. *Surf. Coat. Technol.* **2013**, *220*, 225–231. [[CrossRef](#)]
26. Murthy, J.K.N.; Prasad, K.S.; Gopinath, K.; Venkataraman, B. Characterisation of HVOF sprayed Cr₃C₂-50(Ni20Cr) coating and the influence of binder properties on solid particle erosion behaviour. *Surf. Coat. Technol.* **2010**, *204*, 3975–3985. [[CrossRef](#)]
27. Bergant, Z.; Trdan, U.; Grum, J. Effect of high-temperature furnace treatment on the microstructure and corrosion behavior of NiCrBSi flame-sprayed coatings. *Corros. Sci.* **2014**, *88*, 372–386. [[CrossRef](#)]
28. Laika, A.; Chakravarthy, D.P.; Kale, G.B. On characterisation of wire-arc-plasma-sprayed Ni on alumina substrate. *Mater. Charact.* **2005**, *55*, 118–126. [[CrossRef](#)]
29. Gisario, A.; Puopolo, M.; Venettacci, S.; Veniali, F. Improvement of thermally sprayed WC-Co/NiCr coatings by surface laser processing. *Int. J. Refract. Met. Hard Mater.* **2015**, *52*, 123–130. [[CrossRef](#)]
30. Janka, L.; Norpoth, J.; Eicher, S.; Ripoll, M.R.; Vuoristo, P. Improving the toughness of thermally sprayed Cr₃C₂-NiCr hardmetal coatings by laser post-treatment. *Mater. Des.* **2016**, *98*, 135–142. [[CrossRef](#)]
31. Saedi, S.; Moghaddam, N.S.; Amerinatanzi, A.; Elahinia, M.; Karaca, H.E. On the effects of selective laser melting process parameters on microstructure and thermomechanical response of Ni-rich NiTi. *Acta Mater.* **2018**, *144*, 552–560. [[CrossRef](#)]
32. Yu, J.; Wang, Y.; Zhou, F.; Wang, L.; Pan, Z. Laser remelting of plasma-sprayed nanostructured Al₂O₃-20 wt.% ZrO₂ coatings onto 316L stainless steel. *Appl. Surf. Sci.* **2018**, *431*, 112–121. [[CrossRef](#)]
33. Kromer, R.; Costil, S.; Verdy, C.; Gojon, S.; Liao, H. Laser surface texturing to enhance adhesion bond strength of spray coatings—Cold spraying, wire-arc spraying, and atmospheric plasma spraying. *Surf. Coat. Technol.* **2018**, *352*, 642–653. [[CrossRef](#)]
34. Das, B.; Nath, A.K.; Bandyopadhyay, P.P. Online monitoring of laser remelting of plasma sprayed coatings to study the effect of cooling rate on residual stress and mechanical properties. *Ceram. Int.* **2018**, *44*, 7524–7534. [[CrossRef](#)]
35. Kang, N.; Verdy, C.; Coddet, P.; Xie, Y.; Fu, Y.; Liao, H.; Coddet, C. Effects of laser remelting process on the microstructure, roughness and microhardness of in-situ cold sprayed hypoeutectic Al-Si coating. *Surf. Coat. Technol.* **2017**, *318*, 355–359. [[CrossRef](#)]
36. Benafia, S.; Retraint, D.; Brou, S.Y.; Panicaud, B.; Poussard, J.G. Influence of Surface Mechanical Attrition Treatment on the oxidation behaviour of 316L stainless steel. *Corros. Sci.* **2018**, *136*, 188–200. [[CrossRef](#)]
37. Wang, Z.; Diao, R.; Yuan, Z.; Yu, X.; Fu, T.; Zhao, Y.; Zhan, Z. Surface mechanical attrition treatment and corrosion resistance behavior of TA2 anodic oxide film. *Int. J. Electrochem. Sci.* **2018**, *13*, 4411–4423. [[CrossRef](#)]
38. Nkonta, D.T.; Simescu-Lazar, F.; Drevet, R.; Aaboubi, O.; Fauré, J.; Retraint, D.; Benhayoune, H. Influence of the surface mechanical attrition treatment (SMAT) on the corrosion behavior of Co28Cr6Mo alloy in Ringer's solution. *J. Solid State Electrochem.* **2018**, *22*, 1091–1098. [[CrossRef](#)]
39. Chen, X.H.; Lu, J.; Lu, L.; Lu, K. Tensile properties of a nanocrystalline 316L austenitic stainless steel. *Scr. Mater.* **2005**, *52*, 1039–1044. [[CrossRef](#)]
40. Roland, T.; Retraint, D.; Lu, K.; Lu, J. Generation of nanostructures on 316L stainless steel and its effect on mechanical behavior. *Mater. Sci. Forum* **2005**, *490*, 625–630. [[CrossRef](#)]
41. Uusitalo, J.; Karjalainen, L.P.; Retraint, D.; Palosaari, M. Fatigue properties of steels with ultrasonic attrition treated surface layers. *Mater. Sci. Forum* **2009**, *604–605*, 239–248.
42. Zhou, J.; Sun, Z.; Kanouté, P.; Retraint, D. Effect of surface mechanical attrition treatment on low cycle fatigue properties of an austenitic stainless steel. *Int. J. Fatigue* **2017**, *103*, 309–317. [[CrossRef](#)]
43. Bernoulli, D.; Cao, S.C.; Lu, J.; Dao, M. Enhanced repeated frictional sliding properties in 304 stainless steel with a gradient nanostructured surface. *Surf. Coat. Technol.* **2018**, *339*, 14–19. [[CrossRef](#)]
44. Chamgordani, S.A.; Miresmaeili, R.; Aliofkhaezrai, M. Improvement in tribological behavior of commercial pure titanium (CP-Ti) by surface mechanical attrition treatment (SMAT). *Tribol. Int.* **2018**, *119*, 744–752. [[CrossRef](#)]
45. Liu, Y.; Jin, B.; Li, D.J.; Zeng, X.Q.; Lu, J. Wear behavior of nanocrystalline structured magnesium alloy induced by surface mechanical attrition treatment. *Surf. Coat. Technol.* **2015**, *261*, 219–226. [[CrossRef](#)]
46. Huang, R.; Han, Y. Structure evolution and thermal stability of SMAT-derived nanogained layer on Ti-25Nb-3Mo-3Zr-2Sn alloy at elevated temperatures. *J. Alloy. Compd.* **2013**, *554*, 1–11. [[CrossRef](#)]

47. Liu, Y.; Jin, B.; Lu, J. Mechanical properties and thermal stability of nanocrystallized pure aluminum produced by surface mechanical attrition treatment. *Mater. Sci. Eng. A* **2015**, *636*, 446–451. [[CrossRef](#)]
48. Zhou, J.; Reira, D.; Sun, Z.; Kanouté, P. Comparative study of the effects of surface mechanical attrition treatment and conventional shot peening on low cycle fatigue of a 316L stainless steel. *Surf. Coat. Technol.* **2018**, *349*, 556–566. [[CrossRef](#)]
49. Achache, S.; Lamri, S.; Alhussein, A.; Billard, A.; François, M.; Sanchette, F. Gum Metal thin films obtained by magnetron sputtering of a Ti-Nb-Zr-Ta target. *Mater. Sci. Eng. A* **2016**, *673*, 492–502. [[CrossRef](#)]
50. Jelliti, S.; Richard, C.; Reira, D.; Roland, T.; Chemkhi, M.; Demangel, C. Effect of surface nanocrystallization on the corrosion behavior of Ti–6Al–4V titanium alloy. *Surf. Coat. Technol.* **2013**, *224*, 82–87. [[CrossRef](#)]
51. Zhang, K.; Wang, Z.B. Strain-induced formation of a gradient nanostructured surface layer on an ultrahigh strength bearing steel. *J. Mater. Sci. Technol.* **2018**, *34*, 1676–1684. [[CrossRef](#)]
52. Zhang, H.; Zhao, Y.; Wang, Y.; Yu, H.; Zhang, C. Fabrication of nanostructure in inner-surface of AISI 304 stainless steel pipe with surface plastic deformation. *J. Mater. Sci. Technol.* **2018**, *34*, 2125–2130. [[CrossRef](#)]
53. Zhao, B.; Lv, Y.; Ding, Y.; Wang, L.; Lu, W. The grain refinement mechanisms of various phases in shot-peened Nickel-Aluminum bronze (NAB) alloy. *Mater. Charact.* **2018**, *144*, 77–85. [[CrossRef](#)]
54. Ding, J.; Li, Q.; Li, J.; Xue, S.; Fan, Z.; Wang, H.; Zhang, X. Mechanical behavior of structurally gradient nickel alloy. *Acta Mater.* **2018**, *149*, 57–67. [[CrossRef](#)]
55. Wang, T.G.; Zhao, S.S.; Hua, W.G.; Li, J.B.; Gong, J.; Sun, C. Estimation of residual stress and its effects on the mechanical properties of detonation gun sprayed WC–Co coatings. *Mater. Sci. Eng. A* **2010**, *527*, 454–461. [[CrossRef](#)]
56. Suhonen, T.; Varis, T.; Dosta, S.; Torrell, M.; Guilemany, J.M. Residual stress development in cold sprayed Al, Cu and Ti coatings. *Acta Mater.* **2013**, *61*, 6329–6337. [[CrossRef](#)]
57. Oladijo, O.P.; Venter, A.M.; Cornish, L.A.; Sacks, N. X-ray diffraction measurement of residual stress in WC–Co thermally sprayed coatings onto metal substrates. *Surf. Coat. Technol.* **2012**, *206*, 4725–4729. [[CrossRef](#)]



© 2018 by the authors. Licensee MDPI, Basel, Switzerland. This article is an open access article distributed under the terms and conditions of the Creative Commons Attribution (CC BY) license (<http://creativecommons.org/licenses/by/4.0/>).